Cellular and Molecular Bioengineering, Vol. 1, No. 4, December 2008 *(© 2008)* pp. 263–275
DOI: 10.1007/s12195-008-0030-x

Molecular Interactions

A Nanospring Named Erythrocyte. The Biomembrane Force Probe

CHRISTINE GOURIER, ANTOINE JEGOU, JULIEN HUSSON, and FRÉDÉRIC PINCET

Laboratoire de Physique Statistique de l'Ecole Normale Supérieure, associé aux Universités Paris 6 et Paris 7, UMR CNRS 8550, 24, rue Lhomond, 75231 Paris Cedex 05, France

(Received 29 July 2008; accepted 20 October 2008; published online 11 November 2008)

Abstract—The Biomembrane Force Probe, BFP, is a sensitive technique that allows the quantification of single molecular bonds. It is a versatile tool that can be used in a wide range of forces (0.1 pN to 1 nN) and loading rates ($1–10^6$ pN/s). This article describes the principle of the BFP technique, how to set it up and its various advantages. In order to show that this technique is a powerful tool that can be used on a wide range of systems, two different types of applications are presented. The first example shows how the energy landscape of a single bond can be deduced from the measurements on a well defined pair: the streptavidin–biotin couple. The second example presents a case where cell–cell interactions can be probed at the molecular level: mammalian gametes interactions.

Keywords—Biomembrane Force Probe, Micromanipulation, Single molecular bond, Rupture force, Streptavidin biotin bond, Gamete interactions.

INTRODUCTION

Weak-non covalent interactions govern structural cohesion and mediate most of life's functions. These interactions result from molecular bonds that connect ligands to their receptors. Such ligand receptor complexes can be characterized by the quantification of its strength. The usual way is to exert traction on the complex and measure the pulling force that has to be applied to dissociate it. However, this approach requires in-depth analysis of the measurements. Indeed, ligand-receptors bonds are not covalent, thus weak. Their life spans are short (from microsecond to several days) since they are permanently under thermal fluctuations that will eventually cause their breaking. Let's imagine that a pulling force is applied very slowly to the bond. After a period equal typically to the bond life span, it will break and the measured force will be close to zero because thermal excitation will have provided the necessary work. Suppose now that the traction is applied very quickly to the same bond. In the short period that precedes its rupture, the probability that a thermal fluctuation high enough to dissociate the complex occurs is weak. A higher force will therefore be measured. This shows that speaking of the strength of a bond has no sense if considered independently of the loading rate. Moreover, if an experiment is made twice on a given molecular complex, even if traction conditions are identical, the measured rupture forces will still be different. This is due to the random nature of thermal fluctuations. Thus, a molecular bond cannot be characterized by a single rupture force. Only a distribution of rupture forces at a given traction condition can be obtained. The theoretical description of a bond under an external pulling force is due to Bell in 1978.[3] In 2001, Evans[8] related it to the theory of transient states based on Arrhénius work at the end of the 19th century and derived by Kramer in 1940.[26]

Only a few techniques capable of measuring rupture forces of single molecular bonds are currently available. The small forces (from a few pN to tens of pN) and distances (nm) involved at a molecular level are a real challenge for the experimentalist. A classical technique with such a precision is the Atomic Force Microscope (AFM). An alternative experimental technique is the Biomembrane Force Probe (BFP), a force transducer designed during the nineties by Evan Evans with the aim to probe molecular adhesion and structure at living cell interfaces.[14]

The present article focuses on this BFP technique. The first section will give a detailed description of the set-up and the progression of a typical experiment. In the second section, the BFP technique will be apply to two very different problems. The first one concerns the kinetics of transition of a single non covalent bond from one metastable state to another. The second one is a more biological question, the interactions of mammalian gametes.

Address correspondence to Frédéric Pincet, Laboratoire de Physique Statistique de l'Ecole Normale Supérieure, associé aux Universités Paris 6 et Paris 7, UMR CNRS 8550, 24, rue Lhomond, 75231 Paris Cedex 05, France. Electronic mail: pincet@lps.ens.fr

THE BFP TECHNIQUE

General description

The BFP[14] (Fig. 1) uses a force transducer made of a biotinylated erythrocyte (biotinylated Red Blood Cell, bRBC) maintained by a glass micropipette. A streptavidin-coated glass microbead is attached to the bRBC. The erythrocyte is used as a spring of known stiffness k, which is tuned by the controlled aspiration pressure applied by the holding micropipette: the stronger the aspiration, the higher k. The assembly formed by the bRBC and the microbead constitutes a powerful nanodynamometer and is the force transducer used in the BFP. The streptavidin-coated glass bead can be decorated with ligands of interest which will be displayed on the tip of the force transducer. When the decorated glass bead is brought into contact with a target (another bead, a vesicle, a living cell, etc) bearing complementary receptors, one or more bonds may form. When this situation occurs, an adhesion event is observed. For simplicity, we will simply call it "an event". The density of ligands and/or receptors on the surfaces is generally adjusted to observe an event in less than 10% of contacts. As we will later see, such control is not always possible. In the case of a homogeneous distribution of ligand and/or receptors at the surfaces, such a rate of events ensures a probability higher than 95% that any given event corresponds to a single molecular bond.[29] It is worth noting that the finding that bond formation is a rare event proves that most detected events represent single molecular bonds only if it is assumed that single molecular bonds can actually be detected.

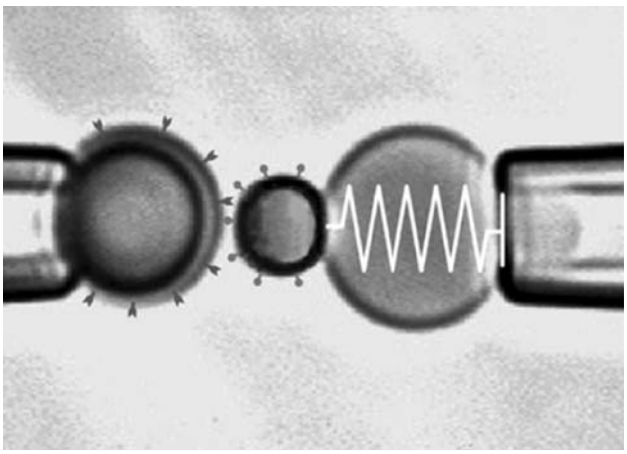

FIGURE 1. ***Right*: probe of the BFP composed by a biotinylated erythrocyte and a streptavidinated glass bead. The red blood cell is used as a spring. Its stiffness is controlled by the aspiration pressure in the holding pipette. The glass bead is also functionalysed with ligands. *Left*: the target (here another bead) decorated with receptors is maintained at the extremity of a second pipette. From Merkel *et al.*[29]**

When the two surfaces are separated, the bond is submitted to a traction force that induces the deformation of the red blood cell. In practice, this deformation is measured through a precise video tracking of the microbead attached to the bRBC. The rupture force of the bond is deduced from the maximum elongation of the red blood cell. As explained above, because of thermal fluctuations, the rupture force depends on the traction conditions and only a distribution of rupture forces can be obtained for any given traction conditions.

Micropipette Fabrication

The BFP technique requires glass micropipettes with inner diameter adapted to the size of the beads, vesicles or cells used (typically from 2 to 10 μm). The different steps of pipette preparation are detailed in Fig. 2. Micropipettes are first obtained by elongating

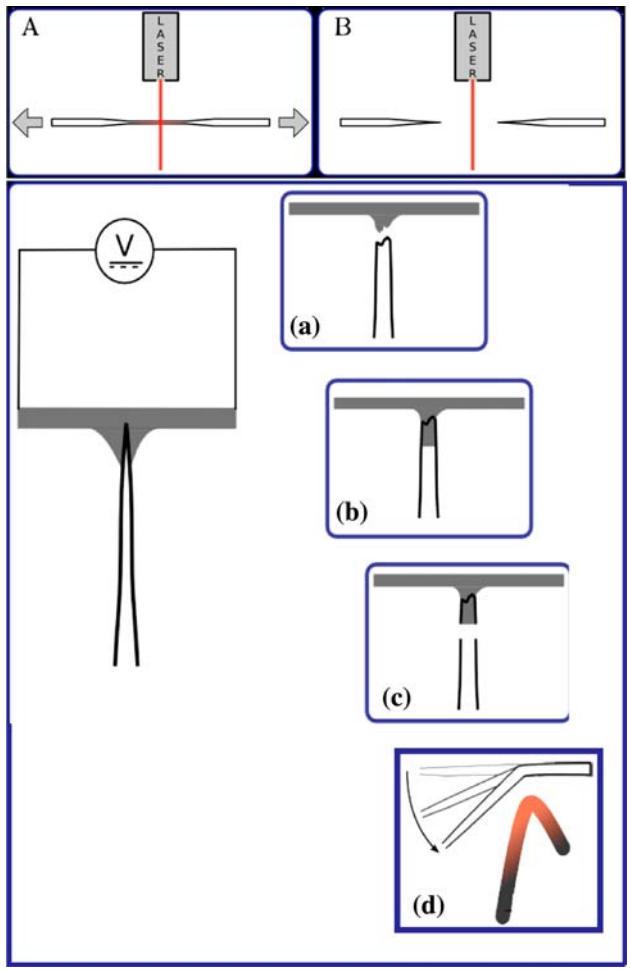

FIGURE 2. Micropipette fabrication. Step 1: elongation of a borosilicate glass capillary with a micropipette puller. Step 2: (a–c) aperture of the micropipette to a suitable diameter with a microforge. Step 3: (d) Tilt of the pipette extremity (necessary for some applications).

borosilicate glass capillaries (1 mm outer diameter, 0.58 mm inner diameter, Harvard Apparatus, USA) with a micropipette puller (P-2000, Sutter Instruments Co., USA). This apparatus is made of a laser used as heating source, and of two pulling springs. The central part of the capillary is heated while the springs apply a traction force to the capillary extremities. The central part of the capillary gets thinner and thinner until it breaks. After breaking, the capillary is split into two closed micropipettes. Next a custom-made microforge allows the opening of the micropipette extremity at the desired diameter. The microforge is made of a platinum wire connected to a power supply. A solid drop of glass fixed on the wire melts when the power is on. The closed tip of the pipette is introduced over a few micrometers into the melted glass before power is switched off. The solidification of the glass drop generates a stress at the extremity of the pipette inducing its rupture. The resulting pipette is open but its aperture is not regular. To circumvent this problem, power is switched on again and the pipette is brought into contact with the melted glass drop a second time. Through capillarity forces, a tongue of melted glass enters the pipette. When power is finally switched off, the pipette breaks in a neat fracture at the end of the tongue.

For some applications, tilted pipettes must be used (see Fig. 2d). In these cases, the extremity of the pipette is brought close to the wire. When power is on, the heat produced by the hot wire force the pipette to bend. Heating is stopped when the tilt angle is satisfactory (typically 30°).

Micromanipulation and Aspiration

Depending on the application, the experiments take place either in a Petri dish filled with adequate medium or in a chamber made of two glass coverslips facing each other where approximately 200 μL of fluid are held by capillary forces (Fig. 3). In this latter case, straight micropipettes enter the chamber from its sides. With a Petri dish, pipettes get into the medium from the top and therefore tilted pipettes are required. In order to avoid cell or bead attachment to their surfaces, the micropipettes and the chamber can be incubated for one hour in a solution (water or buffer) with ~10% Bovine Serum Albumin, and washed several times in experimental chamber before introducing the beads and the cells. Each pipette (generally two, sometimes three) is filled with medium then fixed to micromanipulators mounted on the stage of an inverted microscope (in our case a DMIRB Leica microscope), and connected to homemade manometers for pressure adjustment. The manometers are made of simple reservoirs filled with pure water. If continuity of liquid from the reservoir to the experimental chamber via the micropipette is well established, the difference between the chamber and the reservoir levels allows to induce an aspiration pressure or a superpressure inside the pipette, and therefore to maintain or release the beads or the cells in the chamber.

The experiments were conducted under the microscope (63× leica objective with 1.5 (supplementary lens) equipped with a video device (camera purchased from JAI Corporation, Japan).

The Force Transducer

The Force Transducer Constituents

The force transducer is made of a streptavidin-coated glass microbead attached to a bRBC that is obtained from fresh samples of human red cells that were washed and biotinylated by covalently linking an amine-reactive PEG-biotin polymer (NHS-PEG3400-biotin, Interchim, Montluçon, France) to their surface. bRBCs can be stored in PBS at 4 °C for later use. The streptavidinated microbeads are obtained from uniform silica microspheres (mean diameter 3 or 4 μm, Bangs Laboratories Inc., IN, USA) that were cleaned in a mixture of ammonium hydroxide, hydrogen peroxide, and water at boiling temperature. After several washes in ultrapure water, the glass beads are covalently

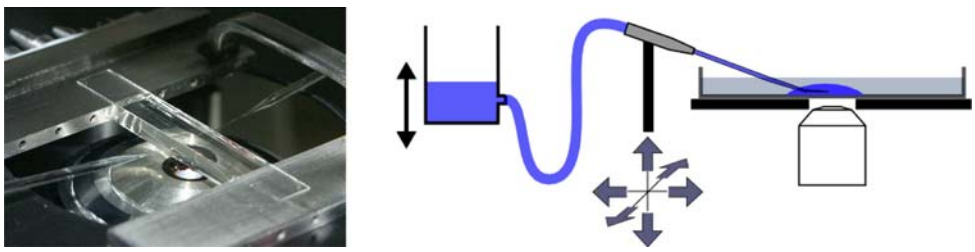

FIGURE 3. Two different experimental chambers: *left*: two glass coverslips facing each other where approximately 200 μL of fluid are held by capillary forces. Straight micropipettes enter the chamber from its sides. *Right*: petri dish. Tilted pipettes get into the medium from the top. Each pipette is filled, fixed to micromanipulators mounted on the stage of an inverted microscope, and connected to reservoirs filled with pure water for pressure adjustment.

bound with amino silane groups (*N*-(2-Aminoethyl)-3-aminopropylmethydimethoxysilane, ABCR GmbH, Germany). The silanized glass beads are then reacted with a mixture of Amine-reactive polyethylene oxide polyethylene glycol with biotin (NHS-NHS-LC-LC-biotin, Interchim, Montluçon, France) and Sulfo-MBS (Pierce, c/o Touzard et Matignon, France). The last step consists in saturating biotinylated microbeads with streptavidin by incubated the beads in a 2 mg/mL streptavidin solution (Jackson Immunoresearch Laboratories, Inc., USA). Beads are finally washed several times in PBS at 4 °C for later use.

Force Transducer Assembling

A crucial step in the preparation of a BFP experiments is the assembling of the force transducer. It is illustrated in Fig. 4. Biotinylated erythrocytes and streptavidinated beads are first introduced in the experimental chamber. With the micromanipulators, the extremities of the two opposite pipettes are brought close to a red blood cell and a bead respectively. If aspiration pressures are imposed to the micropipettes, they grab a bead and an erythrocyte. The red blood cell and the bead are then micromanipulated in contact in a way that both are aligned with the pipette axis. This contact allows the formation of many streptavidin/biotin bonds. When releasing the aspiration pressure in the bead holding pipette, the bead remains firmly attached to the erythrocyte. The high affinity of biotin for streptavidin ensures a long time adhesion compared to a BFP experiment duration (from a few minutes to tens of minutes) and an adhesion stronger than the interactions that are studied.

The Force Transducer Spring Constant

Evans[10] has studied the deformation of a red blood cell submitted to a force. For small deformation (i.e. it will be the case in both applications described later), the erythrocyte behaves like a spring with a spring constant given by Eq. (1):

$$k = \frac{\pi R_p \Delta P}{\left(\ln\left(\frac{2R_g}{R_p}\right) + \ln\left(\frac{2R_g}{r_b}\right)\right)\left(1 - \frac{R_p}{R_g}\right)} \quad (1)$$

where ΔP is the aspiration pressure applied to red blood cell holding pipette, R_p the pipette radius, R_g the red blood cell radius outside the pipette and r_b the radius of the contact area between the red blood cell and the glass bead. The force transducer spring constant k can be easily tuned, even during the course of an experiment, from 10 pN/μm to 10,000 pN/μm by a simple adjustment of the aspiration pressure ΔP. If water continuity between the reservoir and the pipette is ensured in the hydraulic system that controls the pressure, k remains stable with 5% accuracy even at low values. However, the presence of air bubbles will make the aspiration and consequently the spring constant unstable. When the erythrocyte is submitted to an interaction, it is compressed or stretched depending on whether the interaction is repulsive or attractive. This deformation is obtained by tracking the position of the glass bead fixed to the red blood cell. Indeed, when observed with a slightly unfocused optical microscope, the bead displays a light spot with a gaussian intensity profile on its center. This spot is tracked by video processing with the camera connected to the microscope. The tracking procedure developed in the laboratory gives the real time position of the bead at 360 Hz. The difference of the bead position when the red blood cell is at rest and under interaction gives the deformation of the erythrocyte with an accuracy of a few nanometers.

Measurable physical deformation of red blood cells ranges typically from 10 nm to 1 μm. When multiplying it by the spring constant k of the red blood cell, the force exerted on the force transducer is obtained. The forces accessible with the BFP technique are therefore theoretically ranged between 0.1 pN and 10 nN. In practice, the high sensitivity in forces obtained using weak spring constants is limited by the fluctuation of the red blood cell position due to thermal excitation ($\Delta x^2 \sim k_b T/k$). The advantage of a high spring constant is the weak amplitude of position fluctuations,

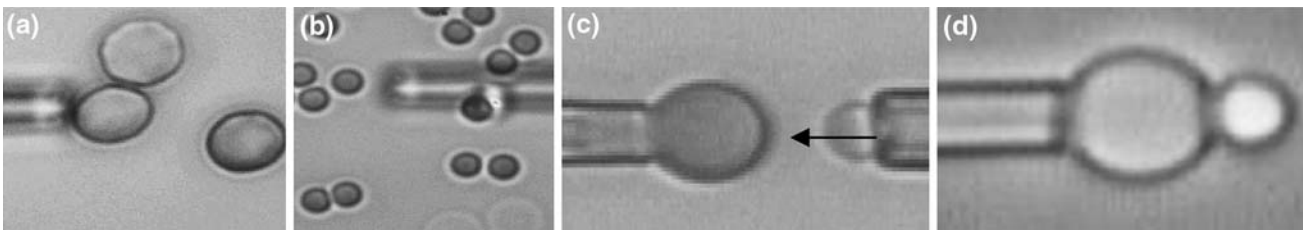

FIGURE 4. Sequences fort the assembling of force transducer. (a) The left pipette grabs a biotinylated red blood cell. (b) the right pipette grabs a streptavidinated glass bead. (c) The bead is brought into contact with the erythrocyte in the alignment of the red blood cell holding pipette. (d) When the aspiration pressure of the bead holding pipette is released, the bead remains firmly attached to the erythrocyte thanks to multiple strepatvidin/biotin bonds.

however the accuracy on the force evaluation becomes poor ($\Delta f^2 \sim k_b Tk$).

The Sequences of a BFP Experiment

The force measurements consist in approach-contact-retraction automatized cycles between the probe functionalized with ligands and the target bearing the receptors.

These cycles are obtained by moving one of the pipettes along its axis towards the other one that remains still. The moving pipette is coupled to a linear piezoelectric translator (Physik Instrumente, Germany) allowing a very fine translation of the pipette at a controlled speed. This piezoelectric translator is connected to a digital-analog converter and a personal computer from which the program controlling the approach-contact-retraction cycles is started.

To detail the sequences of a BFP experiment, let's take for example the case where the pipette holding the target is moving (Fig. 5a) while the force transducer holding pipette remains still. During the approach phase, the target is translated with constant speed into contact with the force transducer. The contact produces a compression of the bRBC detected by tracking the attached bead. When the measured force reaches a chosen compression value (F_{max}, typically a few tens of pN), pipette translation is stopped, and the contact position is maintained during a time lapse imposed by the experimenter (typically hundreds of milliseconds) before the retraction phase begins. During this latter phase, the target is separated from the probe at constant speed v_0. If a bond has been formed, the bead, attached to the target, has to follow its movement when retracted. The red blood cell is elongated in the traction direction until the bond breaks. When the rupture occurs, the probe rapidly comes back to its equilibrium position. This process can also be described in term of forces: until it breaks, the bond is submitted to a traction force which increases as the target is moved back.

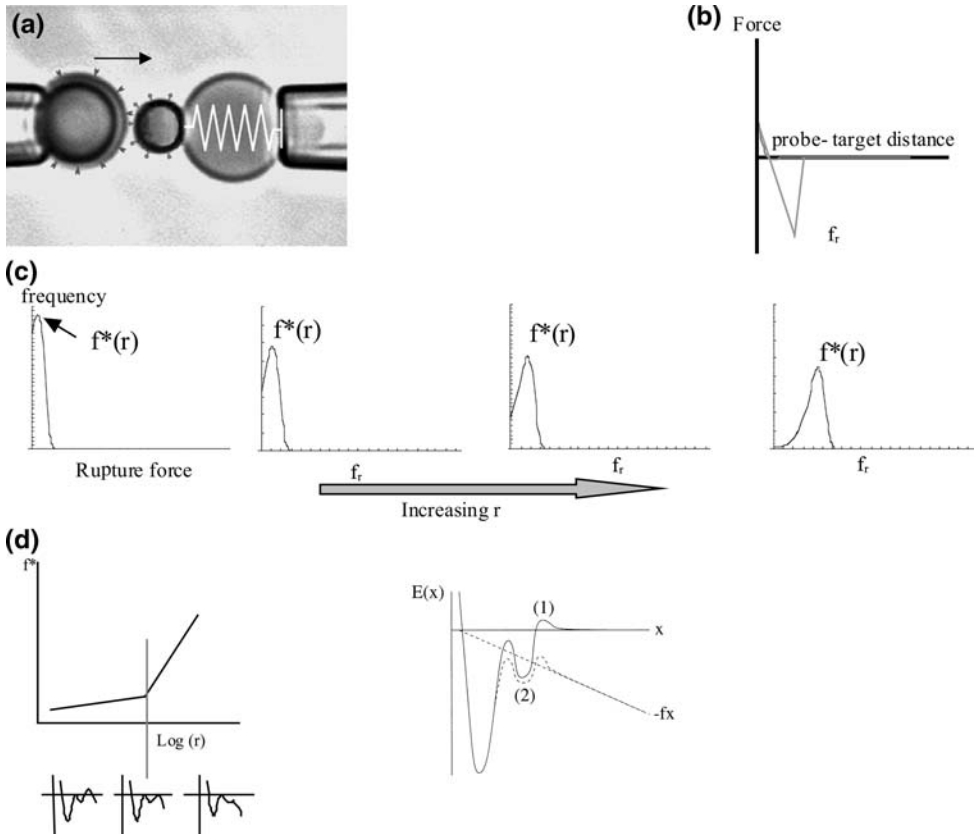

FIGURE 5. (a) The target is brought in contact with the probe. (b) Force distance curve observed when a bond has been formed. Like in an AFM only a relative value of the distance can be obtained. Another technique, the Surface Forces Apparatus (SFA),[27,30] can provide the absolute distance between substrates. In the BFP, after contact is achieved (non zero positive force), the compressibility of the target can be probed. The rupture force of the bond corresponds to the force measured when the ligand/receptor complex dissociates upon a given loading rate. (c) Rupture force distributions of a bond obtained for several loading rates. (d) Dynamic force spectrum of the bond. Each linear regime in the dynamic force spectra corresponds to a given barrier (here 2 barriers) in the energy landscape of the interaction.

The evolution in time of this force is given by $F = (kv_0)t - F_{max}$ where t is the time, starting from the beginning of the retraction phase. Thus, the traction force is a ramp. The slope, $r = kv_0$, is called the loading rate. The rupture force of the bond corresponds to the force measured when the ligand/receptor complex dissociates upon a given loading rate (Fig. 5b). As mentioned above, the strength of the bond is not characterized by a given force but by a force distribution that depends on the loading rate. In the BFP experiments, rupture force distributions of a bond can be obtained for several loading rates (Fig. 5c). For a given loading rate, a high number of approach-retraction-separation cycles must be performed with many probe and target couples in order to obtain statistically significant rupture force histograms. A convenient way of visualizing the robustness of the bond is to plot the most likely rupture force f^* deduced from each force distribution as a function of the logarithm of the loading rate (Fig. 5d). Such a representation is often called a dynamic force spectrum. Dynamic force spectroscopy provides a bridge between rupture forces measurements and the energy landscape of the interaction between two biomolecular objects. Indeed, the energy landscape of a bond displays main energy barriers that the system has to overcome to reach the unbound state (Fig. 5d). Standard dynamic force spectroscopy theory states that each linear regime in the dynamic force semi-log spectra corresponds to a given barrier in the energy landscape of the interaction.[4,12,15,20,28] Even though this assumption has been somewhat shaken recently,[1,22] it can be considered as a first approximation that n different regimes corresponded at most to n different barriers.[7]

For each of them, the relation between f^* and the loading rate is expressed as:

$$f^* = \frac{k_B T}{\Delta x} \mathrm{Ln}\left(\frac{r}{\frac{k_B T}{\Delta x} v_0}\right) \quad (2)$$

Δx corresponds to the distance over which the ligand must be pulled from the receptor in order dissociate the complex. It is therefore the distance between the energetic well in which the system is trapped and the main energy barrier. v_0 is the rate of escape from this well to the unbound state under zero force.

Energies can be deduced from frequencies v_0 by using:

$$v_0 = \frac{1}{t_D} \exp\left(-\frac{\Delta E}{k_B T}\right) \quad (3)$$

where ΔE is the height of the corresponding barrier of the energy landscape and t_D a microscopic time scale of the order of 10^{-10} to 10^{-9} s. Δx and v_0 are obtained by a linear fit of the f^* vs. Log(r).

APPLICATIONS

The Streptavidin Biotin Paradox: A Story of Time[33]

Because of its high affinity as a non-covalent bond, the streptavidin–biotin complex is often used in biology or chemistry to couple molecules. It is also well-known[6,17] and widely studied (see for instance[16,18,23,29,32]). With the BFP technique previously described (the target was a biotinylated glass bead), Evans's group has established rupture force distributions of the streptavidin–biotin complex for several loading rates (Fig. 6),[29] from which for a pulling force of 75 pN, an upper bound for the life span of the bond equal to 75 ms was deduced. This strongly contradicts another work done by Bustamante's group where the life span of the same complex was obtained by a different technique.[2] For their experiment, they use DNA strands whose extremities are functionalized with a biotin on which a streptavidinated latex bead is attached. A controlled traction force is applied to one of the beads through a hydrodynamic flow. The time over which the bead detaches from the DNA provides the life span of the bond. They showed that up to 80 pN, the bonds are stable over one minute which is at least two orders of magnitude higher than the one obtained with the BFP experiment. Hence, one has to reach the senseless conclusion that for a given constant pulling force, the life span of the bond will depend on the technique used to apply the force. This is the streptavidin–biotin paradox. Our study was devoted to understanding its origin.

Let's first focus on another fundamental result related to the streptavidin–biotin complex. Molecular dynamics simulations provide relevant information about the energy landscape of the bond. By simulating the extraction of a biotin out of an avidin binding pocket in half a nanosecond, Schulten's group has been able to completely follow the trajectory of the biotin leading to the bond rupture.[23] From this trajectory, they approximated the neighborhood of the minima in the energy landscape (Fig. 7). This study indicates that there are three minima and therefore also three barriers in the energy landscape. The presence of three barriers is corroborated by an independent experiment in which streptavidin-coated beads rolled on a biotinylated surface in a flow chamber.[32]

With the BFP technique, Evans's group obtained from rupture force distributions of the streptavidin–biotin complex at several loading rates a dynamic force spectrum showing two linear regimes (Fig. 6). We have seen in the previous section that each linear regime corresponds to a given barrier in the energy landscape.[4,12,15,20,28] Thus, in the BFP experiments, only two barriers are observed in the energy landscape

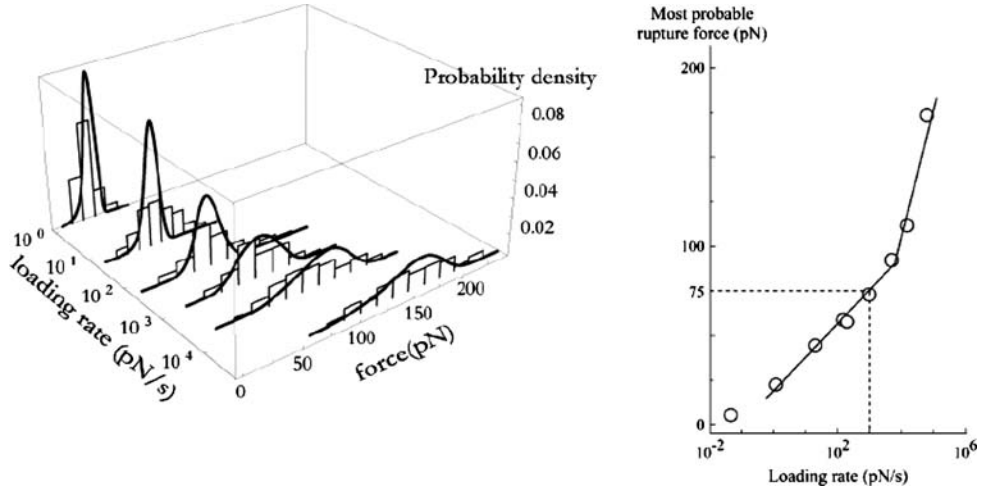

FIGURE 6. ***Left*: Probability density of the rupture force at different loading rates ranged between 1 and 60,000 pN/s obtained from Merkel et al.[29] The associated fits correspond to the distributions expected by applying the Kramers' model (Eq. 4) to the two outer barriers of the energy landscape given Fig. 7. *Right*: Experimental curve obtained by Evans' group of the most likely rupture force of a single streptavidin–biotin bond as a function of the loading rate. Two regimes can be observed as indicated by the two linear slopes.**

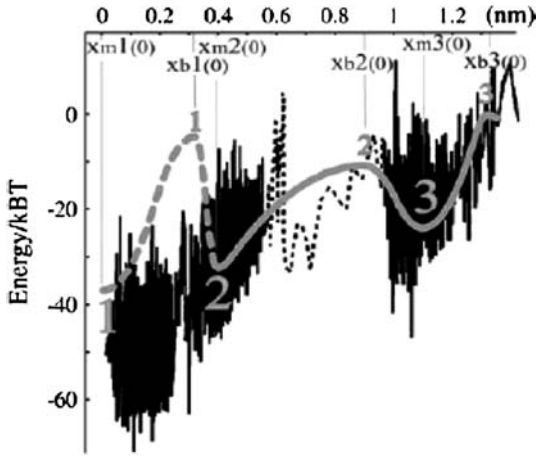

FIGURE 7. Energy landscape of the streptavidin–biotin bond. The landscape used to obtain the probabilities in Fig. 6 (*shaded line*) is superimposed to the one predicted by molecular dynamic simulations (solid lines, given in Merkel et al.[29] and deduced from original data of Shulten's group[23]). The shaded dashed line represents the inmost barrier that is seen in the DNA experiments but not with the BFP measurements. The values $x_m1(0)$, $x_m2(0)$, $x_m3(0)$, $x_b1(0)$, $x_b2(0)$, and $x_b3(0)$, are, respectively, the positions of the first, second, and third minimums and of the first, second, and third barriers under zero force.

of the streptavidin–biotin bond. As molecular dynamics simulations and flow chamber data showed that three barriers are present, one of these barriers is missing in the BFP measurements. In order to determine which one, we have reanalyzed in details the distributions of rupture forces for all the loading rates. These distributions can be theoretically predicted by applying reaction-rate theory, also known as Kramers' theory,[13,19,26] to the energy landscape of the bond. In order to proceed with the analysis, it is necessary to describe this theory in the case where there are two barriers in a one-dimensional energy landscape. The probabilities of being in each of the two energy minima are given by:

$$\frac{dP_1(t)}{dt} = -v_{12}(f)P_1(t) + v_{21}(f)P_2(t)$$
$$\frac{dP_2(t)}{dt} = +v_{12}(f)P_1(t) - v_{21}(f)P_2(t) - v_{23}(f)P_2(t) \quad (4)$$

where $P_1(t)$ and $P_2(t)$ are the probability to be respectively in the first, and second minimum, f is the pulling force which is related to the time t through the loading rate r by $f = $ r.t, and $v_{ij}(f)$ are the transition rates from a minimum i to a neighbor minimum j, 3 referring to the unbound state. We have tried to apply Kramers' theory to each possible pair of barriers of the energy landscape. The only way by which the experimental rupture force distributions obtained by Evans's group could be fitted was by keeping the two outer barriers from the molecular dynamics and assuming that the bond is in the second deepest minimum at the start of the separation process. The predicted rupture force distributions are given in Fig. 6. The agreement with the experimental histograms is almost perfect for all the loading rates. The conclusion is therefore that in the BFP experiment the streptavidin–biotin bond did not reach its deepest minimum. This may be the difference between these measurements and the DNA stretching technique. Intuitively, it can be understood since in the BFP the bond was given a fraction of second to form while for the study with DNA, the

DNA strand had been attached to the streptavidin-coated beads for several minutes before any pulling force was applied. Hence, we can assume that the history of the bond is at the origin of the streptavidin–biotin paradox.

In order to test this assumption we have conducted experiments in which both experimental approaches were combined: we have used the BFP technique with streptavidin-coated beads that had previously been incubated with DNA strands biotinylated on one end (Fig. 8). As the streptavidin–biotin bonds have been formed a long time before the pulling process starts, the rupture forces should be larger than the ones obtained by Evans's group with the BFP also. However, as it is important to make a large number of measurements (a least one hundred per loading rate) to obtain good statistics and smooth distributions, it is necessary to keep the same bead over several approaching-separation cycles. Thus, it may happen that a DNA strand that had previously been detached from the bead reattaches through a newly formed streptavidin–biotin bond. Consequently, the expected distribution should present two peaks: one corresponding to the "old" bonds, like in the DNA stretching studies, and one corresponding to the "new" bonds, like in the previous BFP measurements. This is exactly what we have observed (Fig. 9a). By adding biocytin (0.1 mg/mL) in the solution in order to block all the available streptavidin sites, the first peak disappears confirming that it was due to the formation of new streptavidin/biotin bonds during the measurements (Fig. 9b). The experimental distributions of Fig. 6 can be predicted by Kramer's theory using the complete energy landscape of Fig. 7 with initial conditions in which the probability to be in the deepest minimum is approximately 0.5. Thus, we have been able to probe experimentally unambiguously the presence of the three barriers with our system and completely find the energy landscape of the streptavidin–biotin bond.

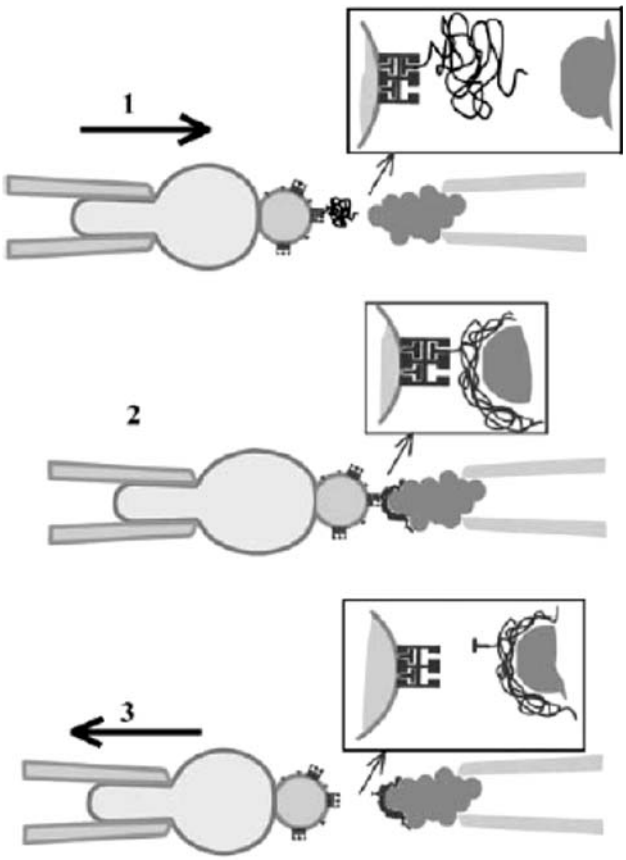

FIGURE 8. Description of the BFP experiment with DNA strands. The streptavidinated glass bead attached to the biotinylated red cell. The DNA is bound to the bead by single streptavidin–biotin bonds. The target is an aggregate of latex particles. When the glass bead and the latex particles are brought in contact, the DNA strongly attaches to the latex particles. Upon separation, the streptavidin–biotin bond is the first one to unbind. This protocol allows the measurements of rupture forces of bonds that have been given several hours to form.

This study using the BFP technique demonstrates that the history of the bond is at the origin of the streptavidin–biotin paradox: in the two contradictory experiments the bond did not reach the same state before a pulling force was applied on it. Our results indicate that the time a system takes to reach equilibrium can be relevant to experimental time scales and may be too often neglected in many fields such as chemistry or biology where association constants are commonly used. There should therefore not only be one association constant per molecular complex but one per metastable state that is relevant in the time scales of the considered process. Of course, the higher the barriers, the longer it takes to fill up the minima.

Mapping Mouse Gamete Interaction Forces Reveal Domains at the Oocyte Membrane with Different Adhesive Properties[24]

Membrane fusion occurs in various biological processes as crucial as transmission of nerve pulse across the synapses, intra-cellular traffic, endo- and exocytosis, fertilization, etc. It is a two-step process which includes adhesion of two membranes followed by their physical merging. Mammalian fertilization offers an example of membrane fusion process that presents several peculiarities: it involves a single couple of heterologous cells, an oocyte and a spermatozoon, isolated within the perivitelline space into which the spermatozoon is the only cell able to penetrate (Fig. 10).

During the last twenty years, investigations have been conducted on mammalian gametes with the aim of

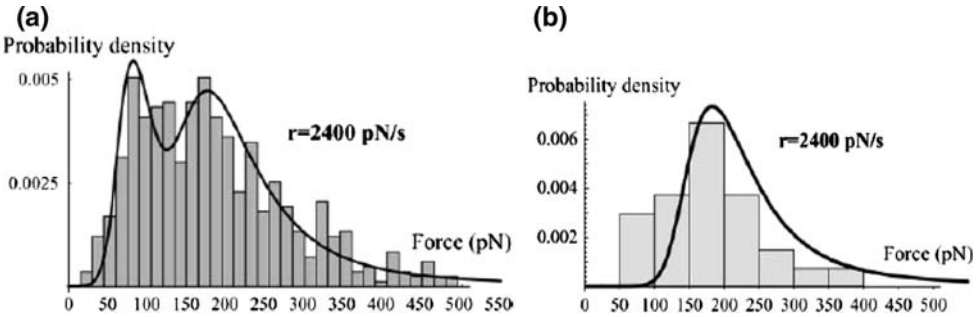

FIGURE 9. Experimental distributions of the rupture force obtained at r = 2400 pN/s, (a) with the DNA coated beads. (b) with the DNA coated beads after adding biocytin in the solution in order to block all the available streptavidin sites. The corresponding probability density of the rupture forces predicted from the energy landscape given in Fig. 7 and Kramers' equations is superimposed.

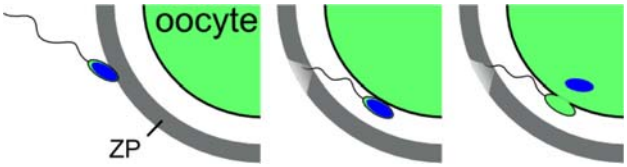

FIGURE 10. sequences of events during gamete fertilization. *Left*: The spermatozoon cross the zona pellucida (ZP) and enters the perivitelline space. *Middle*: Adhesion step of gamete interaction. *Right*: Fusion step of fertilization.

identifying the molecular membrane actors of gamete adhesion and fusion, but also the molecular mechanisms involved in these last and crucial stages of fertilization. The usual biological strategy of investigation of gamete interaction is in vitro insemination experiments performed with wild or genetically modified gametes, in presence or not of targeted antibodies or reagents (for review[9,25,34]). In this context, the BFP technique is an original and powerful tool to quantitatively investigate gamete interaction, very complementary from biological strategies. The idea consists in directly measuring the interaction forces experienced by two isolated gametes (i.e. like what occurs in nature). To adapt the BFP technique to the constraints imposed by the use of two cells as different as an oocyte and a spermatozoon adhering through weak biochemical links, some improvements had been made on the usual set-up described preciously. In mice, oocytes are around 80 μm in diameter and exhibit a pear shape (Fig. 11). A mouse spermatozoon is composed of an almost flat head with dimensions of approximately $5 \times 3 \times 1$ μm^3 and a 60 μm long flagellum.

The main adaptation of the traditional BFP set-up consisted in the fixation of the spermatozoon head on the bead of the BFP transducer. The BFP probe was therefore made of the assembling of a biotinylated erythrocyte, a streptavidinated glass bead, and the spermatozoon, the three components being carefully aligned in the axis of the holding pipette. In addition to the two micropipettes holding respectively the probe and the target (i.e. an oocyte), a third pipette was maintaining the flagellum of the spermatozoon about 20 μm away from its head in order to keep the probe properly aligned. The functional integrity of the cells was maintained by performing all the experiments at 37 °C in a CO_2 independent physiological medium. The approach-contact-retraction cycles of the two gametes were achieved by manoeuvring the oocyte into contact with the spermatozoon head and then pulling on it for separation. The speed and position of the oocyte were controlled all over the approach and traction courses. The contact time of the gametes and maximum compression forces at contact were also controlled. The interaction force felt by the gametes during the whole cycle was continuously obtained. By choosing red blood cell stiffness of 125 pN/μm, a 10 μm/s approach speed of the oocyte holding pipette, and a maximum compression force of 20 pN without pause before the beginning of the retraction phase at 4 μm/s, the total time spent by the cells under compression was around 250 ms. Under these conditions, for 56% of touches no adhesion was detected (Fig. 12a), 18% of gamete contacts gave rise to well-defined single attachment (Fig. 12b, c) and the latest 26 % of touches gave rise to different kinds of interaction, mainly very complex profiles for which multiple attachment points were clearly involved (Fig. 12d). Figure 12 illustrated the typical different shapes of the force distance curves obtained during the separation phase.

Let's focus on the 18% of touches giving single attachment events (Fig. 12b, c). At the start of separation, the oocyte deformation always increases linearly with the force indicating an elastic response to the oocyte's stretching. Then two behaviors are observed: in 11% of the cases the membranes completely separate (Fig. 12c), and in the other 7% there is a transition to a damped regime (Fig. 12b). This second regime corresponds to a viscoelastic behavior of the oocyte

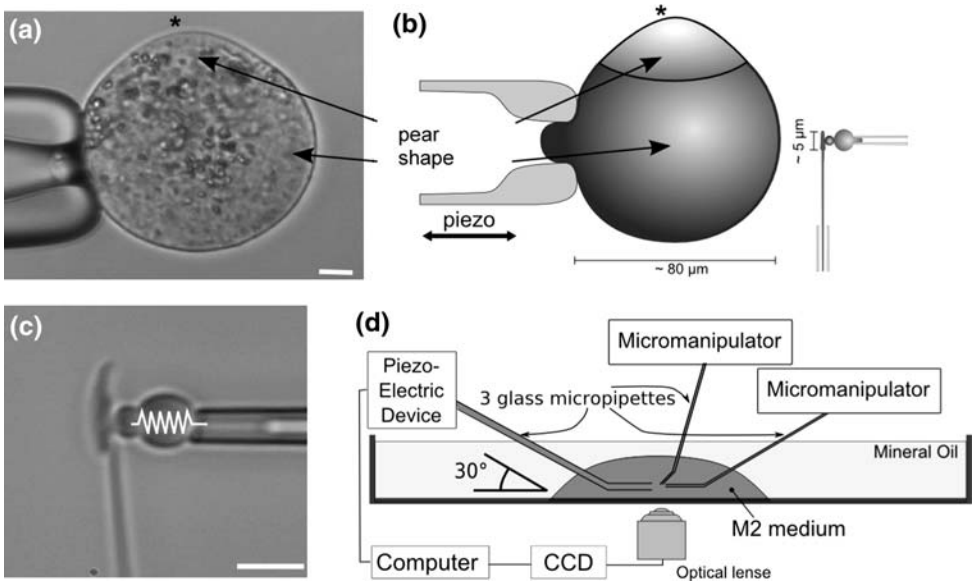

FIGURE 11. Experimental setup. (a) The target is an oocyte held by the left micropipette. The scale bar is 10 μm. (b) Scheme of the relative position of the target and the probe during a BFP experiment. Three glass micropipettes are needed. (c) The probe is made of a red blood cell, a glass bead and a spermatozoon (d) Schematic view of the whole experimental setup. The main drop of M2 medium is under mineral oil to prevent both evaporation at 37 °C and bacterial contamination. Real-time images acquired at 360 images/s by the CCD camera are used to compute the force of the interaction and control the piezo-electric device for precise positioning of the oocyte through online feedback control while the probe is fixed.

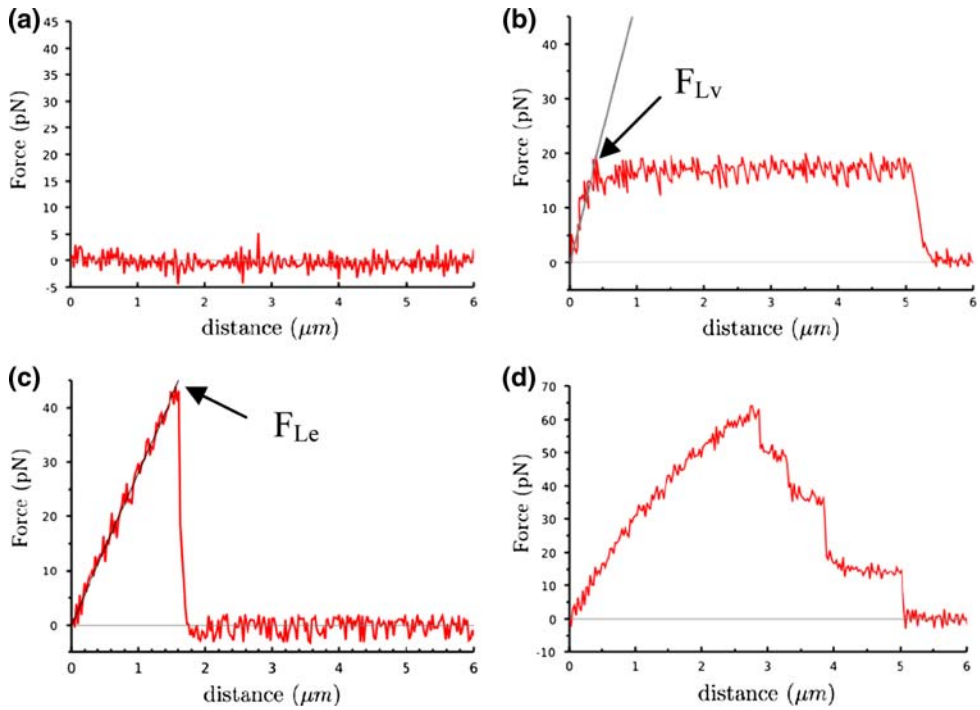

FIGURE 12. Typical force-distance curves of the approach-retraction cycles of the oocyte on the spermatozoon. During the approach phase, the force is zero until the cells are in contact, as revealed by a force increase of up to 20 pN. (a) No attachment between the gamete membranes (b) Single attachment point with elastic behavior and a damped regime: elastic deformation of the oocyte up to a force of F_{Lv}, followed by a transition to a damped regime, with extrusion of a tether from the oocyte membrane. (c) Single attachment point with elastic behavior only. When the cells are separated, the force jumps from a maximum force of F_{Le} to zero. (d) Multiple attachment points: a complex force-distance curve with a succession of force jumps.

plasma membrane associated to the extrusion of a tether. By fluorescent microscopy we showed that these filaments are extruded from the oocyte membrane. Transition from elastic to viscoelastic regime has recently been reported by Evans and coworkers[11,21] on human neutrophils (PMN). According to these authors this transition from the elastic to the viscoelastic regime would be the signature of membrane detachment from the inner cytostructures.

Figure 13 gives the histograms of F_{Le} and F_{Lv} forces corresponding to the end of the linear regime for both types (B and C) of curves under the experimental conditions described above with an effective loading rate of about 100 pN/s. Figure 13a corresponds to the F_{Le} forces obtained for curves without viscoelastic regime. Figure 13b gives the F_{Lv} forces resulting from the curves with two regimes. The shape of the histograms significantly depends on the type of experimental curves. Indeed, the F_{Le} histograms show two distinct force distributions with most probable forces centered close to 8.5 pN and 19.5 pN. By contrast, the F_{Lv} histogram shows a single peak centered around 11 pN. Since the second peak of the F_{Le} histogram corresponds to larger forces than the one involved in F_{Lv} histogram, one can wonder why the oocyte continues to deform elastically even though the traction strength is higher than the threshold forces at which a tether can be extruded. Apparently, exerting a high enough traction force on a strong enough attachment point somewhere on the oocyte is not a sufficient condition to create a tether. The location of the attachment point on the oocyte membrane appears to be a key parameter regarding the capability of the membrane to create a tether. This suggests that the oocyte membrane accessible to the spermatozoon is composed of different kinds of zones with different mechanical characteristics, some of them suitable for tether formation, the others not. In the following the former zones will be referred to v-domains and the latter to e-domains (Fig. 14). When the attachment point between the spermatozoon and the oocyte membrane takes place on a v-domain, the membrane is capable of undergoing a transition from the elastic to the viscoelastic regime. Because of the overlap of F_{Lv} and F_{Le} force distributions, the rupture of the membrane's attachment can also occur in v-domains before any tether is formed, and therefore lead to a purely elastic behavior of the force. In such a case, the experimental force/distance curve is similar to that obtained for membrane contacts occurring in an e-domain (Fig. 12c). Therefore forces, which should have contributed to the F_{Lv} histogram if the attachment point between the gamete membranes had not broken, end up in the lower peak of the F_{Le} histogram (see Fig. 13a). In other words, among the forces obtained at the end of the linear regime for a gamete attachment in a v-domain, a majority composes the F_{Lv} histogram and the rest composes the first peak of the F_{Le} histogram. Only the second peak of the F_{Le} histogram comes from the spermatozoon/oocyte contacts situated in e-domains of the oocyte.

This study has therefore proved the capability of the modified BFP technique used here in quantitatively measuring local changes in gamete membrane adhesion and in probing the mechanical behavior of the oocyte membrane at a micrometer scale. The nature of the e- and v-domains and the molecular players involved in the microvillar and amicrovillar areas of

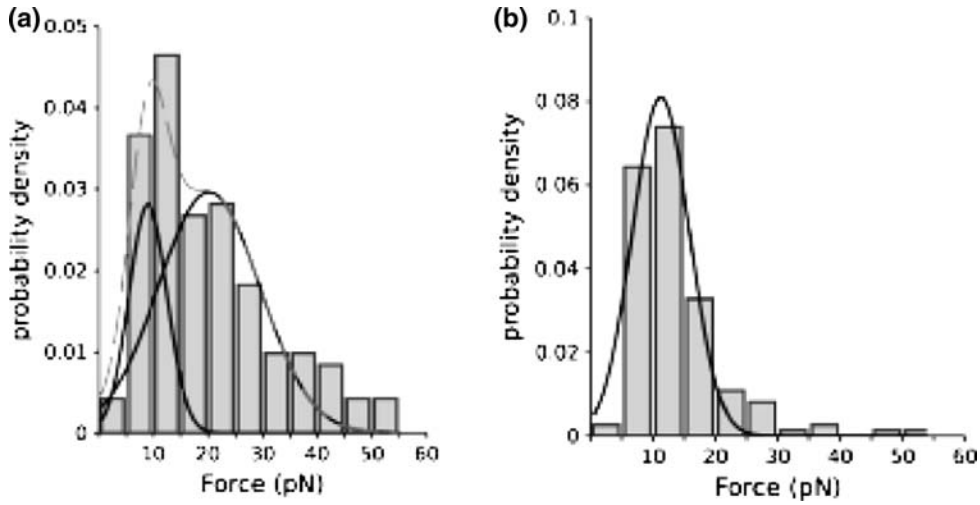

FIGURE 13. Histograms of force distributions for (a) F_{Le} (see Fig. 12c) and (b) F_{Lv} (see Fig. 12b). For F_{Le} distribution, two peaks are shown. The lower peak results from bonds occurring in the v-domain that break before any tether can be formed, and the high-force peak results from bonds occurring in an e-domain of the membrane oocyte.

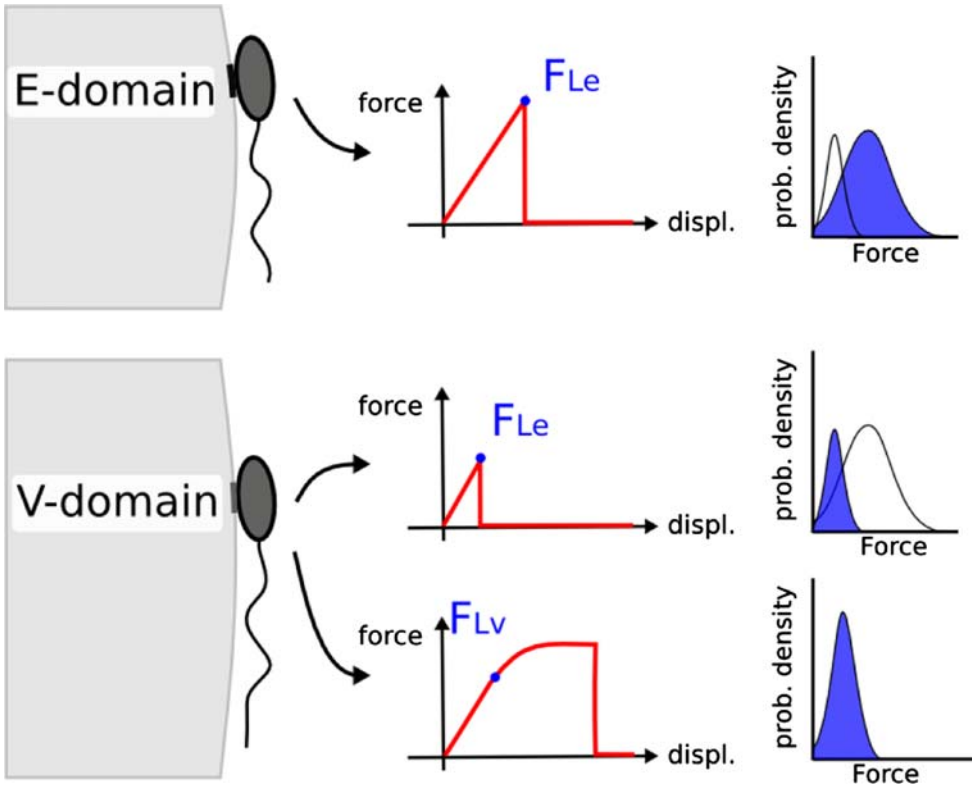

FIGURE 14. v And e domains on the oocyte membrane probed by the spermatozoon. On v-domains, tethers can be extruded after the initial elastic deformation of the oocyte membrane. Two types of curves are therefore obtained depending on whether the bond breaks before or after the extrusion of a tether has occurred. On e-domains, the oocyte can deform only elastically. The curves obtained from v-domains give rise to the F_{Lv} histogram and to the first peak of the F_{Le} histogram. The curves obtained from-domains give rise to the second peak of the F_{Le} histogram.

the oocyte and at the spermatozoon membrane remain to be further investigated. This can be achieved by combining the approach presented here and strategic antibody molecules, knock-out gametes, or drugs modifying the binding between the cell membrane and its cytoskeleton. This approach could therefore become an efficient way of studying the molecular basis of spermatozoon-oocyte plasma membranes interaction during mammalian fertilization, very complementary to the usual biological strategies.[9,25,34] With the latter, it is often impossible to discriminate whether the involved proteins play a role in adhesion, fusion or both steps of fertilization. By contrast, here, gametes adhesion is probed independently from fusion. Moreover, it allows the study of gamete adhesion under conditions close to physiological ones since two isolated gametes are involved the same way as in fertilization.

CONCLUSION

The BFP is a powerful technique that can be used to quantify the strength of a single molecular bond at various levels: from isolated molecules on a substrate to proteins in their natural environment. It is relatively easy to setup. Hence, obtaining force measurement is not the most difficult part. As we have shown on two examples, it takes in-depth and careful analysis to deduce relevant information about the studied system. Often, other approaches such as molecular dynamics simulations or imaging (electron microscopy, confocal microscopy, fluorescence,...) are required to be able to draw conclusions. Even though the BFP is not a commercial technique such as the Atomic Force Microscope (AFM) or flow chamber,[31] it has already been used and modified for various purposes.[5,27]Its versatility should make the BFP a technique that will be more developed in the near future.

REFERENCES

[1]Bartolo, D., I. Derenyi, and A. Ajdari. Dynamic response of adhesion complexes: beyond the single-path picture. *Physi. Rev. E (Stat. Nonlinear Soft Matter Phys.)* 65:051910, 2002.

[2]Baumann, C. G., S. B. Smith, V. A. Bloomfield, and C. Bustamante. Ionic effects on the elasticity of single DNA molecules. *PNAS* 94:6185–6190, 1997.

[3]Bell, G. I. Models for specific adhesion of cells to cells. *Science* 200:618–627, 1978.
[4]Chen, S. Q., and T. A. Springer. Selectin receptor-ligand bonds: Formation limited by shear rate and dissociation governed by the Bell model. *Proc. Natl. Acad. Sci. USA* 98:950–955, 2001.
[5]Chen, W., V. I. Zarnitsyna, K. K. Sarangapani, J. Huang, and C. Zhu. Measuring receptor-ligand binding kinetics on cell surfaces: from adhesion frequency to thermal fluctuation methods. *Cell. Mol. Bioeng*. 2008. doi:10.1007/s12195-008-0024-8.
[6]Chilkoti, A., T. Boland, B. D. Ratner, and P. S. Stayton. The relationship between ligand-binding thermodynamics and protein-ligand interaction forces measured by atomic force microscopy. *Biophys. J.* 69:2125–2130, 1995.
[7]Derenyi, I., D. Bartolo, and A. Ajdari. Effects of intermediate bound states in dynamic force spectroscopy. *Biophys. J.* 86:1263–1269, 2004.
[8]Evans, E. Probing the relation between force—Lifetime—and chemistry in single molecular bonds. *Ann. Rev. Biophys. Biomol. Struct*. 30:105–128, 2001.
[9]Evans, J. P The molecular basis of sperm-oocyte membrane interactions during mammalian fertilization. *Human Reprod. Update* 8:297–311, 2002.
[10]Evans, E., D. Berk, and A. Leung. Detachment of agglutinin-bonded red blood cells. I. Forces to rupture molecular-point attachments. *Biophys. J.* 59:838–848, 1991.
[11]Evans, E., V. Heinrich, A. Leung, and K. Kinoshita. Nano- to microscale dynamics of P-selectin detachment from leukocyte interfaces. I. Membrane separation from the cytoskeleton. *Biophys. J.* 88:2288–2298, 2005.
[12]Evans, E., and F. Ludwig. Dynamic strengths of molecular anchoring and material cohesion in fluid biomembranes. *J. Phys.-Condens. Matter* 12:A315–A320, 2000.
[13]Evans, E., and K. Ritchie. Dynamic strength of molecular adhesion bonds. *Biophys. J.* 72:1541–1555, 1997.
[14]Evans, E., K. Ritchie, and R. Merkel. Sensitive force technique to probe molecular adhesion and structural linkages at biological interfaces. *Biophys. J.* 68:2580–2587, 1995.
[15]Evans, E., and P. M. Williams. Dynamic force spectroscopy. In: Physics of Bio-Molecules, Cells, edited by F. Julicher, P. Ormos, F. David, and H. Flyvbjerg. Berlin, Germany: Springer Verlag, 2002, pp. 145–204.
[16]Florin, E. L., V. T. Moy, and H. E. Gaub. Adhesion forces between individual ligand-receptor Pairs. *Science* 264:415–417, 1994.
[17]Green, N. M. Avidin. *Adv. Protein Chem*. 29:85–133, 1975.
[18]Grubmüller, H., B. Heymann, and P. Tavan. Ligand binding: molecular mechanics calculation of the streptavidin–biotin rupture force. *Science* 271:997–999, 1996.
[19]Hanggi, P., P. Talkner, and M. Borkovec. Reaction-rate theory—50 years after Kramers. *Rev. Modern Phys*. 62: 251–341, 1990.
[20]Hanley, W., O. McCarty, S. Jadhav, Y. Tseng, D. Wirtz, and K. Konstantopoulos. Single molecule characterization of P-selectin/ligand binding. *J. Biol. Chem*. 278:10556–10561, 2003.
[21]Heinrich, V., A. Leung, and E. Evans. Nano- to microscale dynamics of P-selectin detachment from leukocyte interfaces. II. Tether flow terminated by P-selectin dissociation from PSGL-1. *Biophys. J.* 88:2299–2308, 2005.
[22]Hummer, G., and A. Szabo. Kinetics from nonequilibrium single-molecule pulling experiments. *Biophys. J.* 85:5–15, 2003.
[23]Izrailev, S., S. Stepaniants, M. Balsera, Y. Oono, and K. Schulten. Molecular dynamics study of unbinding of the avidin–biotin complex. *Biophys. J.* 72:1568–1581, 1997.
[24]Jegou, A., F. Pincet, E. Perez, J. P. Wolf, A. Ziyyat, and C. Gourier. Mapping mouse gamete interaction forces reveal several oocyte membrane regions with different mechanical and adhesive properties. *Langmuir* 24:1451–1458, 2008.
[25]Kaji, K., and A. Kudo. The mechanism of sperm-oocyte fusion in mammals. *Reproduction* 127:423–429, 2004.
[26]Kramers, H. A. Brownian motion in a field of force and the diffusion model of chemical reactions. *Physica (Utrecht)* 7:284–304, 1940.
[27]Leckband, D. From single molecules to living cells: nanomechanical measurements of cell adhesion. *Cell. Mol. Bioeng*. 2008. doi:10.1007/s12195-008-0029-3.
[28]Li, F. Y., S. D. Redick, H. P. Erickson, and V. T. Moy. Force measurements of the a_5b_1 integrin–fibronectin interaction. *Biophys. J.* 84:1252–1262, 2003.
[29]Merkel, R., P. Nassoy, A. Leung, K. Ritchie, and E. Evans. Energy landscapes of receptor-ligand bonds explored with dynamic force spectroscopy. *Nature* 397:50–53, 1999.
[30]Perez, E., F. Li, D. Tareste, and F. Pincet. The surface force apparatus to reveal the energetics of biomolecules assembly. Application to DNA bases pairing and SNARE fusion proteins folding. *Cell. Mol. Bioeng*. 2008. doi:10.1007/s12195-008-0025-7.
[31]Pierres, A., A.-M. Benoliel, and P. Bongrand. Studying molecular interactions at the single bond level with a laminar flow chamber. *Cell. Mol. Bioeng*. 2008. doi:10.1007/s12195-008-0031-9.
[32]Pierres, A., D. Touchard, A.-M. Benoliel, and P. Bongrand. Dissecting streptavidin–biotin interaction with a laminar flow chamber. *Biophys. J.* 82:3214–3223, 2002.
[33]Pincet, F., and J. Husson. The solution to the streptavidin–biotin paradox: the influence of history on the strength of single molecular bonds. *Biophys. J.* 89:4374–4381, 2005.
[34]Rubinstein, E., A. Ziyyat, J. P. Wolf, F. Le Naour, and C. Boucheix. The molecular players of sperm-egg fusion in mammals. *Semin. Cell. Dev. Biol*. 17:254–263, 2006.